

CRASHWORTHINESS PERFORMANCE OF OPTIMIZED AUXETIC FOAM-
FILLED TUBES UNDER AXIAL LOADINGS

SAEID MOHSENIZADEH

A thesis submitted in fulfilment of the
requirements for the award of the degree of
Doctor of Philosophy

School of Mechanical Engineering
Faculty of Engineering
Universiti Teknologi Malaysia

SEPTEMBER 2019

DEDICATION

To my beloved parents, brother and wife

ACKNOWLEDGEMENT

Foremost, I would like to express my deep and sincere gratitude to my supervisors, Assoc. Prof. Ir. Dr. Zaini Ahmad, Assoc. Prof. Dr. Amran Alias and Dr. Rohah A. Majid for their motivation, enthusiasm, invaluable guidance and continuous supports throughout the duration of my study. Their guidance helped me all through the time of the research and the writing of this thesis as they have always been available to advise me and provide assistance in numerous ways.

Apart from this, I would like to thank the Computational Solid Mechanic Laboratory (CSMLab) members who have shared valuable knowledge with me generously. I also wish to express my warm and sincere thanks to Ph.D. candidate Shuaibu Balogun Alani for his support during the compilation of this thesis.

Last but not least, special thanks goes to my darling parents, brother and wife for giving me moral and cheering supports and care throughout my study in UTM.

ABSTRACT

Filling thin-walled tubes with foam cores is a typical method to promote a desirable energy absorption performance and stabilize the crushing responses of thin-walled tubes under impact loading. Auxetic foams as new class of cellular materials have recently gained popularity within the research community due to their enhanced mechanical properties. However, the energy absorption performance of auxetic foam-filled tubes design information is very limited. The aim of this study is to evaluate the crush response, the energy absorption capacity and the deformation behavior of auxetic foam-filled square and circular tubes under quasi-static and dynamic axial loadings. For comparison, energy absorption performance of empty and conventional foam-filled square and circular tubes was also experimentally and numerically examined with respect to deformation modes and load-displacement responses. All tube specimens were crushed at a constant loading rate of 3 mm/min for quasi-static loading and an initial impact velocity of 5 m/s was adopted for dynamic loading. In order to investigate the influence of tube effective parameters such as wall thickness, diameter, width and height, a series of parametric studies were conducted using validated finite element (FE) models. The initial finding reveals that both auxetic foam-filled square and circular tubes are superior to empty and conventional foam-filled tubes in terms of energy absorption capacity without a significant increase in the initial peak load. From the initial finding and due to the great potential of auxetic foam as cores, a new fabrication technique called Quasi Tri-axial Compression Method (QTCM) was developed to fabricate the auxetic foam with the maximum achievable negative Poisson's ratio. The fabricated auxetic foam with optimal re-entrancy was then introduced as the core for the tubes. Moreover, energy absorption capacity of auxetic foam-filled tubes was experimentally quantified with the foam Poisson's ratio ranging from -0.13 to -0.32. The results show that the energy absorbed by auxetic foam-filled square and circular tubes loaded dynamically are approximately 34.7% and 22% greater than that of conventional foam-filled square and circular tubes respectively. This is practically beneficial when higher kinetic energy needs to be absorbed in order to reduce the impact force transmitted to the occupant's compartment. Furthermore, it is evident that an increase in the auxeticity level of foam filler enhances crashworthiness performance of filled tubes under both quasi-static and dynamic loading conditions. Above all, the primary outcome of this thesis is a design guideline for the use of an auxetic foam as a core for energy absorbing devices where axial impact loading is anticipated.

ABSTRAK

Pengisian tiub berdinding nipis dengan teras busa adalah satu kaedah yang biasa digunakan untuk menghasilkan prestasi penyerapan tenaga yang dikehendaki dan menstabilkan tindak balas remuk tiub berdinding nipis di bawah bebanan hentaman. Busa *auxetic* sebagai kelas baru bahan bersel, baru-baru ini telah mendapat populariti di kalangan komuniti penyelidikan disebabkan oleh sifat-sifat mekanikal yang dipertingkatkan. Walaupun begitu, maklumat reka bentuk ke atas prestasi penyerapan bagi tiub terisi dengan busa *auxetic* adalah amat terhad. Tujuan kajian ini adalah untuk menilai tindak balas remuk, kapasiti penyerapan tenaga dan kelakuan ubahbentuk bagi tiub berbentuk segi empat sama dan bulat terisi dengan busa *auxetic* di bawah keadaan bebanan kuasi-statik dan dinamik. Sebagai perbandingan, prestasi penyerapan tenaga tiub kosong dan tiub terisi dengan busa konvensional telah juga diperiksa secara eksperimen dan numerik terhadap mod ubah bentuk dan tindak balas beban-anjakan. Semua spesimen tiub telah diremukkan pada kadar bebanan tetap iaitu 3 mm/min bagi bebanan kuasi-statik dan pada halaju awal hentaman iaitu 5 m/s bagi bebanan dinamik. Untuk menyiasat pengaruh parameter-parameter tiub yang berkesan seperti ketebalan dinding, diameter, lebar dan ketinggian, satu siri kajian parametrik telah dijalankan dengan menggunakan model unsur terhingga (FE) yang telah disahkan. Penemuan awal menunjukkan bahawa kedua-dua tiub berbentuk segi empat sama dan bulat terisi dengan busa *auxetic* adalah lebih baik daripada tiub yang kosong dan tiub yang terisi dengan busa konvensional dari segi kapasiti penyerapan tenaga tanpa peningkatan beban puncak awal yang ketara. Dari penemuan awal dan potensi terbaik busa *auxetic* sebagai teras, satu teknik fabrikasi baru dinamakan Kaedah Kuasi Pemampatan Tri-paksi (QTCM) telah dibangunkan untuk menghasilkan busa *auxetic* dengan nisbah Poisson negatif maksimum yang boleh dicapai. Busa *auxetic* yang dihasilkan dengan *re-entrancy* optimum kemudiannya telah diperkenalkan sebagai teras untuk tiub. Selain daripada itu, kapasiti penyerapan tenaga bagi tiub terisi dengan busa *auxetic* telah ditentukan secara eksperimen dengan nisbah Poisson busa berjulat dari -0.13 hingga -0.32. Keputusan menunjukkan bahawa tenaga yang diserap oleh tiub segi empat sama dan bulat yang terisi dengan busa *auxetic* yang dibebani secara dinamik adalah masing-masing kira-kira 34.7% dan 22% lebih tinggi daripada tiub segi empat sama dan bulat yang terisi dengan busa konvensional. Ini adalah berfaedah secara praktikalnya apabila tenaga kinetik yang lebih tinggi perlu diserap untuk mengurangkan daya hentaman yang dipindahkan kepada ruang penghuni. Tambahan lagi, ianya jelas bahawa peningkatan tahap *auxeticity* bagi pengisi busa dapat meningkatkan prestasi tiub terisi di bawah kedua-dua keadaan bebanan kuasi-statik dan dinamik. Secara keseluruhannya, hasil utama tesis ini adalah satu garis panduan reka bentuk untuk penggunaan busa *auxetic* sebagai teras bagi peranti penyerapan tenaga yang mana beban hentaman adalah dijangkakan.

TABLE OF CONTENTS

	TITLE	PAGE
	DECLARATION	ii
	DEDICATION	iii
	ACKNOWLEDGEMENT	iv
	ABSTRACT	v
	ABSTRAK	vi
	TABLE OF CONTENTS	vii
	LIST OF TABLES	xiii
	LIST OF FIGURES	xv
	LIST OF ABBREVIATIONS	xxiv
	LIST OF SYMBOLS	xxvi
CHAPTER 1	INTRODUCTION	1
	1.1 Background of Research	1
	1.2 Problem Statement	5
	1.3 Research Objectives	6
	1.4 Research Scopes	7
	1.5 Significance of Research	9
	1.6 Outline of the Thesis	10
CHAPTER 2	LITERATURE REVIEW	11
	2.1 Introduction	11
	2.2 Structural Impact and Crashworthiness	11
	2.3 Crashworthiness Criteria	13
	2.3.1 Energy Absorption and Mean Crushing Force	14
	2.3.2 Crush Force Efficiency	15
	2.3.3 Specific Energy Absorption	16
	2.4 Load Characterizations	17
	2.4.1 Load Scenario	17

2.4.2	Loading Rate	18
2.5	Thin-walled Tubes	19
2.5.1	Deformation Profiles of Square and Circular Tubes under Axial Loading	22
2.6	Foam Materials	26
2.6.1	The In-Plane Properties of Cellular Structure under Uniaxial Compression	28
2.7	Foam-filled Thin-walled Tubes	31
2.7.1	Interaction Effect	34
2.8	Auxetic Materials	38
2.8.1	History of Auxetic Materials	38
2.8.2	Converting Methods for Polymeric Foam	39
2.8.2.1	Solvent-Based Fabrication Process	40
2.8.2.2	Multi-Phase Fabrication Process	41
2.8.2.3	Carbon Dioxide Assisted Auxetic Fabrication	42
2.8.2.4	Hydro-Mechanical Auxetic Fabrication	44
2.8.3	Influencing Parameter in Conversion Process	45
2.8.3.1	Influence of Heating Temperature	45
2.8.3.2	Influence of Heating Time	47
2.8.3.3	Influence of Cell Size	48
2.8.3.4	Influence of Volumetric Compression Ratio	49
2.8.3.5	Cooling Process	50
2.8.4	Mechanical Properties of Auxetic Foam	51
2.8.4.1	Indentation of Auxetic Foam	51
2.8.4.2	Toughness	52
2.8.5	Application of Auxetic Materials	54
2.9	Summary	55
CHAPTER 3	RESEARCH METHODOLOGY	57
3.1	Introduction	57
3.2	Material Characterization	58

3.2.1	Conventional Polymeric Foams	58
3.2.2	Fabrication Process of Auxetic Foam	59
3.2.3	Thin-walled Tubular Structures	61
3.3	Experiment	62
3.3.1	Specimens Preparation	62
3.3.2	Experimental Techniques	63
3.3.2.1	Tensile Test	63
3.3.2.2	Compression Test	70
3.3.2.3	Poisson's Ratio Measurement	71
3.3.2.4	Quasi-Static Test	74
3.3.2.5	Dynamic Test	75
3.4	Finite Element Analysis	76
3.4.1	FE Discretization	77
3.4.2	Mesh Refinement	78
3.4.3	Material Model	82
3.4.4	Boundary Conditions, Loading and Interaction	83
3.4.5	Validation of Quasi-Static Condition	85
3.4.6	Control and Stability	87
CHAPTER 4	AN INITIAL STUDY ON THE ENERGY ABSORPTION CAPABILITY OF AUXETIC FOAM-FILLED SQUARE TUBE	89
4.1	Introduction	89
4.2	Material Preparation and Experimental Procedure	89
4.2.1	Fabrication Process of Foams	89
4.2.2	Specimens Preparation	91
4.3	Experimental Results and Validation of the FE Model	92
4.3.1	Deformation Mode and Force-Displacement Response	92
4.3.2	Energy Absorption and Mean Crushing Force Responses	94
4.3.3	Initial Peak Load and Second Peak Load	96
4.3.4	Crush Force Efficiency	97
4.3.5	Specific Energy Absorption	98

	4.3.6	Comparison The Effect of Density and Poisson's Ratio of Foam Core On the Energy Absorption Performance	99
	4.3.7	Validation of FE Model	100
	4.4	Summary	102
CHAPTER 5		FABRICATION OF OPTIMIZED AUXETIC FOAM	103
	5.1	Introduction	103
	5.2	Material Specification	103
	5.3	Fabrication Procedure for Auxetic Foam	105
	5.3.1	SDP Estimation in Different Directions	106
	5.3.2	Effect of SDP on Volumetric Compression Process	111
	5.3.3	Volumetric Compression	113
	5.3.4	Heating and Cooling Processes	114
	5.3.5	Heating Time and Temperature	116
	5.4	Specification of Produced Auxetic Foams	118
	5.5	Morphology of Fabricated Auxetic Foam	120
	5.6	Summary	122
CHAPTER 6		QUASI-STATIC AND DYNAMIC RESPONSES OF FOAM-FILLED TUBES UNDER AXIAL LOADING	125
	6.1	Introduction	125
	6.2	Auxetic Foam for Square Tube	125
	6.2.1	Specimens Preparation	125
	6.2.2	Experimental Tests	127
	6.2.3	Deformation Shapes and Load-Displacement Responses	129
	6.2.4	Crushing Characteristics and Energy Absorption Efficiency of Auxetic Foam-Filled Square Tubes	129
	6.2.4.1	Energy Absorption Response	129
	6.2.4.2	Mean Crushing Force Response	131
	6.2.4.3	Initial Peak Load Response	132

6.2.4.4	Crush Force Efficiency Response	133
6.2.4.5	Specific Energy Absorption Responses	134
6.2.5	Comparison Between Quasi-Static and Dynamic Responses	137
6.2.6	Influence of Foam Core on Crushing Characteristic and Deformation Mode of Square Tube	139
6.2.7	Influence of Foam Poisson's Ratio on the Interaction Effect	143
6.2.8	Validation Results for ET, CFFT and AFFT3 under Quasi-Static Loading	145
6.2.9	Influence of Geometrical Parameters on Energy Absorption Performance	149
6.2.9.1	Influence of Wall Thickness	149
6.2.9.2	Influence of Auxetic Foam on the Crashworthiness Performance	151
6.2.9.3	Influence of Tube Width	153
6.2.9.4	Influence of Tube Height	158
6.3	Auxetic Foam for Circular Tube	161
6.3.1	Specimens Preparation	161
6.3.2	Deformation Profile and Crush Behavior Characteristics	162
6.3.3	Energy Absorption (<i>EA</i>) and Mean Crushing Force (<i>MCF</i>)	167
6.3.4	Crush Force Efficiency; <i>CFE</i>	169
6.3.5	Influence of NPR on the Interaction Effect	169
6.3.6	Validation Result for AFFCT under Compressive Axial Loading	171
6.3.7	Collapse Profiles of AFFCT	173
6.3.7.1	Influence of Wall Thickness on the Collapse Profile	174
6.3.7.2	Influence of Auxetic Foam on the Collapse Profile	177
6.3.7.3	Influence of Tube Diameter on the Collapse Profile	179
6.4	Summary	180

CHAPTER 7	CONCLUSIONS AND RECOMMENDATIONS	183
7.1	Concluding Remarks	183
7.2	Recommendations for Future Work	186
REFERENCES		187
LIST OF PUBLICATION		197

LIST OF TABLES

TABLE NO.	TITLE	PAGE
Table 2.1	<i>MCF</i> for foam-filled tubes	36
Table 2.2	Converting method for polymeric foam	45
Table 2.3	Summary of the applications of the auxetic materials [24, 108, 127-131]	55
Table 3.1	Tube dimensions	62
Table 3.2	Mechanical properties of aluminum tubes	67
Table 3.3	True stress versus plastic strain for square aluminum alloy in the FE model	82
Table 3.4	True stress versus plastic strain for circular aluminum alloy in the FE model	83
Table 3.5	Material model for crushable foam (MAT_CRUSHABLE_FOAM)	83
Table 4.1	Mechanical properties of foams	91
Table 4.2	Experimental results from quasi-static test	98
Table 4.3	Specification of fabricated foams	99
Table 5.1	Specification of conventional polymeric close-cell foams	105
Table 5.2	Maximum allowable compressive strain in different directions	112
Table 5.3	A comparison of the theoretical maximum <i>VCRs</i> of different types of foam	113
Table 5.4	Investigation of the softening temperature and heating time of samples	115
Table 5.5	Specification of converted auxetic foams	118
Table 6.1	Foam specification	126
Table 6.2	Specimen types	127
Table 6.3	Energy absorption capability of filled tubes specimens under axial loading	136
Table 6.4	Fold wavelengths	143

Table 6.5	Experimental results from axial compressive loads of foam core	144
Table 6.6	Energy absorption of foam-filled tubes and the sum of the EA of foam core and ET	145
Table 6.7	Dimensions of the models used in the FE analysis	149
Table 6.8	Simulation results for ET, CFFT and AFFT3 in different wall thicknesses	152
Table 6.9	Geometrical parameters of square tube	153
Table 6.10	Geometrical parameters of square tube	159
Table 6.11	Specimen types	162
Table 6.12	Geometrical parameters of circular tube	174

LIST OF FIGURES

FIGURE NO.	TITLE	PAGE
Figure 1.1	Crash boxes as an energy absorbing system [4]	1
Figure 1.2	Schematic behavior of material with (a) PPR, (b) ZPR and (c) NPR [25]	3
Figure 1.3	Schematic deformation profile (indentation resistance) of (a) non-auxetic and (b) auxetic materials [25]	4
Figure 2.1	Crush characteristics of structural crashworthiness [40].	13
Figure 2.2	Crashworthiness terminology	14
Figure 2.3	Triggered square tube [14] and corrugated circular tube [44].	16
Figure 2.4	Typical loading on the automobile's energy absorbing devices in collision [46]	18
Figure 2.5	Plastic deformation of circular tubes under (a) quasi-static and (b) dynamic axial loadings [37]	19
Figure 2.6	Progressive buckling of (a) circular and (b) square tubes when loaded axially [59]	20
Figure 2.7	(a) Honeycomb, (b) polymeric and (c) metallic foam-filled tubes and (d) double-cell tubular profile [51, 62, 63]	20
Figure 2.8	Thin-walled tube configurations; (a) cylindrical, (b) square prism, (c) rectangular prism, (d) frusta, (e) Pyramidal and (f) triangular prism [52]	21
Figure 2.9	Tube configuration and deformation shape for (a) star-shaped and (b) equilateral triangular cross-sections tubes [42, 66]	22
Figure 2.10	Global bending profiles of (a) square tube [70] and (b) circular tube [71] under axial loading	23
Figure 2.11	Collapse profiles of circular tubes in various tube lengths (TL) when subjected to dynamic load [74]	24
Figure 2.12	Various deformation profiles of square tubes under axial loading [1]	25
Figure 2.13	Various deformation profiles for circular tubes under axial loading; (a) axisymmetric, (b) non-axisymmetric and (c) mixed modes [71]	26

Figure 2.14	Mode classification plot of cylindrical tubes under axial loading [71]	26
Figure 2.15	(a) Polyurethane foam and (b) aluminum foam [75]	27
Figure 2.16	Opened-cell [33, 76] and closed-cell foams [76, 77]	27
Figure 2.17	A uniformed unit cell of a hexagonal honeycomb structure [78]	28
Figure 2.18	Schematic stress-strain curve for elastomeric cellular structures compressed in the y direction [78]	29
Figure 2.19	<i>MCF</i> for various types of material and geometrical parameters [2]	32
Figure 2.20	Effect of foam density on the (a) fold length and (b) specific energy absorption of polystyrene foam-filled circular tube under quasi-static axial loading [64]	33
Figure 2.21	Comparison of (a) collapse profile and (b) mean crushing force-displacement curve for circular empty and cork-filled tubes [89]	33
Figure 2.22	Deformation profile for empty and foam-filled tubes under different loading conditions [43]	35
Figure 2.23	Crush force versus displacement curve of foam-filled aluminium tube [92]	36
Figure 2.24	Deformation profile for (a) empty tube, (b) aluminum honeycomb-filled tube (c) and polyurethane foam-filled tubes. Comparison of load-displacement curves for (d) foam, empty tube, sum of the foam and empty tube and foam-filled tube and (e) aluminum honeycomb, empty tube, sum of the honeycomb and empty tube and honeycomb-filled tube [51]	37
Figure 2.25	Deformation behaviors of materials with (a) positive and (b) negative Poisson's ratios [104]	39
Figure 2.26	Microstructure of (a) conventional foam, (b) fabricated auxetic foam using chemo-mechanical process and (c) fabricated auxetic foam using thermo-mechanical process [33]	41
Figure 2.27	Tangent modulus versus Poisson's ratio of foam samples (conventional, 1st auxetic, reverted and 2nd auxetic) subjected to (a) compressive and (b) tensile loading [105]	42
Figure 2.28	Energy dissipation versus Poisson's ratio of foam samples (conventional, 1st auxetic, reverted and 2nd auxetic) subjected to (a) compressive and (b) tensile loading [105]	42

Figure 2. 29	(a) Schematic diagram of experimental set-up and (b) mechanism for structural conversion in polyurethane foam during auxetic conversion [32]	43
Figure 2.30	Different steps of converting process; (a) wrapping, (b) Thick-walled cylinder and immersing the wrapped sample in hydraulic oil, (c) applying hydrostatic pressure, (d) molding, (e) heating [110]	44
Figure 2.31	Schematic diagram of the measurement of foam softening temperature [30]	46
Figure 2.32	Diagram indicating different time-temperature profiles for auxetic fabrication reported by researchers	48
Figure 2.33	Contour map of 100 PPI Polymeric foams fabricated in different conditions [109]	49
Figure 2.34	Indentation behavior of (a) conventional (non-auxetic) and (b) auxetic materials	52
Figure 2.35	Energy absorbed per unit volume versus (a) compression and (b) tensile stresses for various <i>VCR</i> [28]	53
Figure 2.36	Smart filter to demonstrate the variable permeability [122].	54
Figure 2. 37	Dilator employing an auxetic end sheath [25, 126]	55
Figure 3.1	Overall research methodology flowchart	58
Figure 3.2	Conventional foam block	59
Figure 3.3	(a) Steel cubic mold and (b) steel mold caps	60
Figure 3.4	(a) Applying compressive load in <i>x</i> , <i>y</i> and <i>z</i> directions, (b) molding process and (c) heating operation in the preheated oven	60
Figure 3.5	Tube geometry: (a) square and (b) circular tubes	61
Figure 3.6	Tube configurations and foam fillers	62
Figure 3.7	Tensile test samples form (a) circular and (b) square cross-section tubes	64
Figure 3.8	Designed grips of tensile test sample for: (a) curve (circular tube) and (b) flat (square tube) form	64
Figure 3.9	(a) Schematic gripping technique of tensile test sample and (b) tensile test set-up	65
Figure 3.10	(a) Gripped flat plate test sample and (b) tensile test set-up	66

Figure 3.11	Stress-strain curves of aluminum tubes; (a) square and (b) circular	66
Figure 3.12	Tensile test sample	67
Figure 3.13	(a) Tensile test set-up, (b) loading process and (c) end of test	68
Figure 3.14	Tested samples	68
Figure 3.15	Tensile stress-strain curve for (a) CCF35 and (b) CCF45	69
Figure 3.16	Tensile stress-strain curve for (a) AF35 and (b) AF45	70
Figure 3.17	(a) Foam samples and (b) compression test set-up	71
Figure 3.18	Schematic diagram for measuring foam Poisson's ratio. (a) Foam sample and (b) test set-up	73
Figure 3.19	Poisson's ratio measurement set-up	74
Figure 3.20	Schematic diagram of the test sample undergoing axial compressive loading in y direction, (a) an unloaded test sample, (b) conventional and (c) auxetic foam	74
Figure 3.21	Quasi-static test set-up	75
Figure 3.22	Drop weight impact test machine	76
Figure 3.23	FE modeling flowchart	77
Figure 3.24	Geometrical model, tube dimension, loading and boundary condition arrangement of FE model for foam-filled tube	78
Figure 3.25	Mesh refinement study for aluminum empty tube when the element size varies from 5 mm to 0.5 mm	79
Figure 3.26	Verification of mesh element size for aluminum empty tube based on convergence of (a) initial peak load versus element size and (b) energy absorption versus element size	80
Figure 3.27	Mesh refinement study for foam-filled tube when the element size of foam core varies from 6 mm to 2 mm	80
Figure 3.28	Verification of mesh element size for foam-filled tube based on convergence of (a) initial peak load versus element size and (b) energy absorption versus element size	81
Figure 3.29	Finalized meshed model; (a) Tube ES=1 mm (b) Foam ES=2.5 mm	81
Figure 3.30	Velocity time-history for the rigid movable mass used in quasi-static simulation	84

Figure 3. 31	(a) Load-displacement curve and (b) energy absorption-displacement response at different loading velocities. (c) Energy curve in quasi-static simulation	86
Figure 3.32	Orthogonal section views of FE model for foam-filled square tube	87
Figure 4.1	Steps of polyurethane foam fabrication; (a)weighing the chemical compounds, (b) mixing and filling the mold, (c) capping the mold	90
Figure 4.2	Stress–strain curves of; (a) conventional and (b) auxetic foams	91
Figure 4.3	Tube configurations; (a) CFFT and (c) AFFT	92
Figure 4.4	Deformation mode; (a) CFFT and (b) AFFT	93
Figure 4.5	Quasi-static load-displacement response for CFFT and AFFT	94
Figure 4.6	(a) Energy absorption-displacement response and (b) mean crushing force-displacement response for CFFT and AFFT	95
Figure 4.7	(a) Initial peak load and (b) second peak load for CFFT and AFFT under quasi-static loading condition	96
Figure 4.8	Comparison of crush force efficiency of ET, CFFT and AFFT from the existing experimental results	97
Figure 4.9	Comparison of specific energy absorption of ET, CFFT and AFFT from the existing experimental results	98
Figure 4.10	Conventional and auxetic foam with approximately the same density	99
Figure 4.11	Comparison between CFFT and AFFT; (a) <i>EA</i> and (b) <i>SEA</i> in additional experiments	100
Figure 4.12	Experimental and numerical deformed profiles of AFFT under axial loading	101
Figure 4.13	Experimental vs. numerical; (a) load-displacement curves and (b) absorbed energy responses versus displacement	101
Figure 4.14	Comparison of load response of experimental result and predicted FE simulation; (a) initial peak load and (b) mean crushing force	102
Figure 5.1	Compressive stress-strain curves of conventional foam in three directions for (a) CCF35 and (b) CCF45	104
Figure 5.2	Overall fabrication methodology	106

Figure 5.3	Schematic diagrams of the volumetric compression process in three different directions (a) x , (b) y and (c) z	107
Figure 5.4	A new design of compression test rig (a) press and mold, (b) impactors and (c) mold caps	108
Figure 5.5	Compression loading to determine SDP in x direction; (a) foam sample, (b) molding and (c) loading process	108
Figure 5.6	(a) Stress-strain curve of foam in x direction, (b) G-clamp and mold and (c) observation of foam cell structure using optical microscope	109
Figure 5.7	Compression loading to determine SDP in y and z directions; (a) compressing virgin foam by cap in x direction, (b) extract stress-strain curve in y direction, (c) compressing virgin foam in two (x and y) directions and (d) extract stress-strain curve in z direction	110
Figure 5.8	Compressive stress-strain curves in x , y and z directions to determine the SDPs (a) CCF35 and (b) CCF45	111
Figure 5.9	Volumetric compression to fabricate the auxetic foam; (a) compressing to SDPs in x , y and z directions and (b) molding for the heating process	114
Figure 5.10	(a) Measurement of heating time and (b) heating process	115
Figure 5.11	The temperature-time profiles of the uncompressed and compressed samples heated in the oven for (a) CCF35 and (b) CCF45	117
Figure 5.12	Auxetic samples produced by the proposed methodology in this study	117
Figure 5.13	Compressive stress-strain curves in three directions (a) AF35 and (b) AF45	119
Figure 5.14	A comparison between elastic region of conventional and auxetic foams; (a) CCF35 and AF35, (b) CCF45 and AF45	120
Figure 5.15	SEM images of CCF35 in three directions; (a) x , (b) y and (c) z at 50 magnification	121
Figure 5.16	SEM images of AF35 in three directions; (a) x , (b) y and (c) z at 50 magnification	121
Figure 5.17	SEM images of CCF45 in three directions; (a) x , (b) y and (c) z at 50 magnification	122
Figure 5.18	SEM images of AF45 in three directions; (a) x , (b) y and (c) z at 50 magnification	122

Figure 6.1	Foam types: (a) conventional, (b) AX1, (c) AX2 and (d) AX3 foam	126
Figure 6.2	Tube configuration (a) CON-filled tube (CFFT), (b) AX1-filled tube (AFFT1), (c) AX2-filled tube (AFFT2) and (d) AX3-filled tube (AFFT3)	127
Figure 6.3	Deformation modes for (a) CFFT, (b) AFFT1, (c) AFFT2 and (d) AFFT3 under quasi-static and dynamic axial loading conditions	128
Figure 6.4	Load-displacement response of specimens subjected to (a) quasi-static and (b) dynamic axial loadings	128
Figure 6.5	Comparison of EA versus displacement curves; (a) quasi-static and (b) dynamic loadings	130
Figure 6.6	Comparison of MCF versus displacement curves; (a) quasi-static and (b) dynamic loadings	132
Figure 6.7	Effect of foam Poisson's ratio on the initial peak load of specimens in (a) quasi-static and (b) dynamic loadings	133
Figure 6.8	Comparison the CFE of specimens in (a) quasi-static and (b) dynamic loadings	134
Figure 6.9	Comparison of SEA versus displacement curves (a) quasi-static and (b) dynamic loadings	136
Figure 6.10	Comparison between quasi-static and dynamic force-deflection curves for (a) ET, (b) CFFT, (c) AFFT1, (d) AFFT2 and (e) AFFT3	137
Figure 6.11	Comparison of crush responses of empty and filled tubes under quasi-static and dynamic loadings; (a) EA (b) SEA and (c) CFE	138
Figure 6.12	Cutting section of crushed specimens; (a) ET, (b) CFFT and (c) AFFT3	141
Figure 6.13	Inward penetration length of tube walls in (a) conventional and (b) auxetic foams	141
Figure 6.14	Schematic diagram of folded square tube with inward fold wavelength (F_i) and outward fold wavelength (F_o)	142
Figure 6.15	(a) Compression test set-up and (b) load versus deflection curves of foams	144
Figure 6.16	Comparison of absorbed energy for (a) ET+CON and CFFT, (b) ET+AX1 and AFFT1, (c) ET+AX2 and AFFT2, (d) ET+AX3 and AFFT3	145
Figure 6.17	Cont'd Comparison of deformed shapes, load displacement curves and EA versus displacement curves	

	of experimental results and present FE simulations: (a) ET, (b) CFFT and (c) AFFT3	148
Figure 6.18	Tube effective parameters	148
Figure 6.19	Influence of wall thickness on the crush response of ET, CFFT and AFFT3: (a) EA , (b) MCF , (c) P_{max} and (d) CFE	150
Figure 6.20	(a) Energy absorption responses of ET and CFFT for various wall thicknesses. (b) Comparing the P_{max} and (c) CFE of ET, CFFT and AFFT3 with a tube wall thicknesses of 0.98, 0.9 and 0.8, respectively	152
Figure 6.21	Deformation profiles for ET and AFFT3 where the tube width (w) is equal to (a) $0.75 w_0$, (b) w_0 , (c) $1.25 w_0$, (d) $1.5 w_0$ and (e) $1.75 w_0$	154
Figure 6.22	MCF and EA versus displacement curves for ET and AFFT3 where the tube width (w) is equal to (a) $0.75 w_0$, (b) w_0 , (c) $1.25 w_0$, (d) $1.5 w_0$ and (e) $1.75 w_0$	155
Figure 6.23	Influence of tube width variation on the crush responses of ET and AFFT3; (a) energy absorption and (b) specific energy absorption	156
Figure 6.24	Influence of tube width variation on the crush response of ET and AFFT3; (a) initial peak load and (b) crush force efficiency	158
Figure 6.25	Influence of tube height on the crushing response of ET and AFFT3; (a) energy absorption, (b) specific energy absorption and (c) crush force efficiency	160
Figure 6.26	Influence of tube height on the plastic deformation mode of ET tube with the heights of (a) h_0 and (b) $2h_0$	161
Figure 6.27	Circular tube configuration (a) ECT (b) CFFCT and (c) AFFCT	162
Figure 6.28	Deformation profile for ECT, CFFCT and AFFCT under quasi-static and dynamic axial loading	163
Figure 6.29	Load-displacement responses of specimens under (a) quasi-static and (b) dynamic axial loading	164
Figure 6.30	Comparison between the P_{max} of specimens in (a) quasi-static and (b) dynamic axial loading	165
Figure 6.31	Comparison between the mean crush load for formation of each lobe for ECT, CFFCT and AFFCT	166
Figure 6.32	Comparison of EA versus displacement curves; (a) quasi-static and (b) dynamic loading	167

Figure 6.33	Comparison of <i>MCF</i> versus displacement curves; (a) quasi-static and (b) dynamic loadings	168
Figure 6.34	Comparing the <i>CFE</i> of specimens in (a) quasi-static and (b) dynamic loadings	169
Figure 6.35	(a) Compression test set-up and (b) load versus displacement curves for conventional and auxetic foams	170
Figure 6.36	Comparison of absorbed energy for (a) ECT+CON and CFFCT, (b) ECT+AX3 and AFFCT	170
Figure 6. 37	Schematic deformation profile of auxetic foam-filled tube	171
Figure 6.38	Comparison between experimental and numerical results for AFFCT; (a) collapse profiles, (b) load-displacement curves and (c) <i>EA</i> versus displacement curves	172
Figure 6.39	Circular tube effective parameters	173
Figure 6.40	A half-sectional view of a AFFCT under compressive axial crushing	173
Figure 6.41	Influence of wall thickness on the collapse profile of ECT and AFFCT when the wall thickness varies from 0.4 mm to 1 mm	175
Figure 6.42	Comparison of the absorbed energy responses of ECT and AFFCT at different tube wall thicknesses	177
Figure 6.43	Crushing sequences of ECT and AFFCT under quasi-static axial loading	178
Figure 6.44	Influence of auxetic foam on the generated lobes and fold length	179
Figure 6.45	Tube geometries and their geometrical parameters	179
Figure 6.46	Influence of tube diameter on the collapse profile of AFFCT	180

LIST OF ABBREVIATIONS

AFFCT	-	Auxetic Foam-Filled Circular Tube
AFFT	-	Auxetic Foam-Filled Tube
CCF35	-	Conventional polymeric Closed-cell Foam; density 35 kg/m ³
CCF45	-	Conventional polymeric Closed-cell Foam; density 45 kg/m ³
<i>CFE</i>	-	Crush Force Efficiency
CFFCT	-	Conventional Foam-Filled Circular Tube
CFFT	-	Conventional Foam-Filled Tube
<i>CL</i>	-	Crushing Level
CON	-	Conventional foam
<i>EA</i>	-	Energy Absorption
ECT	-	Empty Circular Tube
<i>ES</i>	-	Element Size
ET	-	Empty Tube
FE	-	Finite Element
FEA	-	Finite Element Analysis
<i>H</i>	-	Hardness
<i>IPL</i>	-	Inward Penetration Length
<i>L_{cr}</i>	-	Critical length
LVDT	-	Linear Variable Displacement Transducer
MACS	-	Maximum Allowable Compressive Strain
<i>MCF</i>	-	Mean Crushing Force
<i>MCL</i>	-	Mean Crushing Load
NPR	-	Negative Poisson's Ratio
<i>P_{max}</i>	-	Initial Peak Load
PPI	-	Pores Per Inch
PPR	-	Positive Poisson's Ratio
<i>P_s</i>	-	Second Peak Load
QTCM	-	Quasi Tri-axial Compression Method
SDP	-	Starting Densification Point
<i>SEA</i>	-	Specific Energy Absorption

- TL* - Tube length
- UTM - Universal Testing Machine
- VCR* - Volumetric Compression Ratio

LIST OF SYMBOLS

d	-	Diameter
d_0	-	Initial diameter
E	-	Young's modulus
ε	-	Strain
ε_{Axial}	-	Axial strain
ε_{Eng}	-	Engineering strain
ε_f	-	Fracture strain
$\varepsilon_{Lateral}$	-	Lateral strain
E_p	-	Plateau modulus
ε_{True}	-	True strain
F	-	Crushing force
h	-	Height
h_0	-	Initial height
I	-	Second moment inertia
m	-	Mass
n	-	Rotational stiffness
P_{cr}	-	Critical load
t	-	Thickness
t_0	-	Initial thickness
V	-	volume
V_0	-	Initial volume
w	-	Width
w_0	-	Initial width
δ	-	Crushing length
ν	-	Poisson's ratio
ρ	-	Density
σ_{el}	-	Elastic collapse stress
σ_{el}	-	Elastic collapse stress
σ_{Eng}	-	Engineering stress
σ_{pl}	-	Plastic collapse stress

σ_{True}	-	True stress
σ_u	-	Ultimate tensile stress
σ_y	-	Initial yield stress
σ_{ys}	-	Yield stress

CHAPTER 1

INTRODUCTION

1.1 Background of Research

Increased interest in vehicle safety and crashworthiness has led to considerable investigations on energy absorption capability, crush response, and progressive collapse mode of energy absorbing devices from experimental, analytical and numerical points of view [1-3]. Thin-walled tubular structures as an effective energy absorbing devices have been impressively considered in structural impact applications for mitigating adverse effect of impact with controllable deformation. Therefore, thin-walled tubes have been extensively utilized in automobile industry since they are excellent at dissipating kinetic energy by progressive plastic deformation when subjected to different loading conditions. For instance, as indicated in Figure 1.1, crash boxes in automobile chassis are used for protecting the vehicle's structure and the occupants in the event of impact.

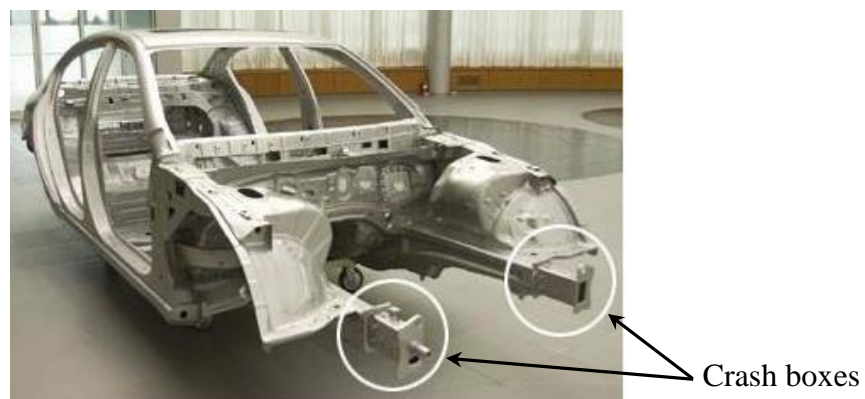


Figure 1.1 Crash boxes as an energy absorbing system [4]

In general, principal factors like structural geometry, materials and loading conditions influence energy absorption capability of thin-walled structures remarkably. Hence, some beneficial numerical and experimental studies have been conducted to

determine crashworthy characteristic of thin-walled tubes of various cross-sections under different loading conditions [5-7].

For many decades, progressive collapse mechanism and folding deformation of thin-walled tubes of various cross-sections have been widely investigated to figure out which cross-section could provide optimum crashworthiness performance [8, 9]. Crushing behavior and deformation modes of circular, rectangular, square, triangular, pyramidal, hexagonal and conical tubes under compressive axial loading were studied. Results of a study carried out by Nia and Parsapour [7], indicated that the cylindrical and triangular tubes exhibit the highest and lowest energy absorption capacity under compressive axial loading respectively.

Despite all modifications done to enhance crashworthiness efficiency of thin-walled structures, crush analysis and crashworthy response of foam-filled thin-walled tubes demonstrate greater energy dissipation, higher collapse resistance and fewer tendency to global bending than empty tubes [2, 10, 11]. Hence, crush response analysis of foam-filled tubes when loaded statically and dynamically has received increased attention in the literature [12, 13]. Accordingly, metallic and non-metallic foams have drawn extensive attention as fillers due to their good energy dissipation performance (since they can withstand large deformation when the load is kept constant). In an investigation on the crush and energy absorption responses of foam-filled extruded aluminum square tube under dynamic and quasi-static axial loading, Hanssen et al. [14] observed that introducing foam filler causes two changes in the crushing mode which are: increase in the number of fold and shorter fold length. Asavavisithchai et al. [15] compared energy absorption capability of foam-filled and empty circular tubes of different length when subjected to static axial load. They also investigated the energy absorbed by foam-filled tube, foam and empty tube individually. The results reveal that due to interaction effect, the sum of the absorbed energy of foam and empty tube is less than the absorbed energy by foam-filled tube. In addition, existence of foam in the tube structure alters the diamond mode of empty tube to concertina mode. Recently, Othman et al. [16] found that introducing polymeric foam into the composite pultruded square tube enhances specific energy absorption and crush force efficiency of pultruded tubes when subjected to quasi-static axial

crushing. In a numerical parametric study, Ahmad and Thambiratnam [17, 18] found that inserting foam filler inside a conical tube may improve the collapse mode and crushing stability of a structure, resulting in greater crashworthiness performance under both oblique and axial loadings in the dynamic and quasi-static loading cases.

In general, the density of foam filler is the most effective factor that controls deformation mode and crush response behavior of foam-filled tube subjected to impact loading. In other words, increasing the density of foam promotes energy absorption capability of foam-filled tubes [19, 20]. However, very high density of foam filler may cause many undesirable crushing characteristics such as global Euler buckling, premature tensile rupture and low weight effectiveness which greatly decrease the energy absorption capacity of filled structures [10, 21]. Reid et al. [10] observed that, global Euler buckling occurred when polymeric foam of density over 320 kg/m^3 was inserted into square tube. Onsalung et al. [20] conducted a comparative experimental investigation on crush analysis of square tube filled with polymeric foam with densities 200 kg/m^3 and 300 kg/m^3 , and discovered that specific energy absorption of filled tube is great when foam density 200 kg/m^3 is used.

Most foam materials inserted in the tubes have a level of capacity to absorb energy. One of the most common specifications is to have positive Poisson's ratio (PPR) or zero Poisson's ratio (ZPR). It is worth noting that the shearing effect is nearly zero for foam materials with ZPR. In recent decade, a special interest has been shown in invention of foams with negative Poisson's ratio (NPR). Such foam materials that exhibit NPR are termed auxetic [22, 23]. Auxetic materials show an opposite behavior in which lateral expansion occurs during the longitudinal stretch and vice versa [24]. Figure 1.2 demonstrates the schematic deformation of material with PPR, ZPR and NPR under tensile strain.

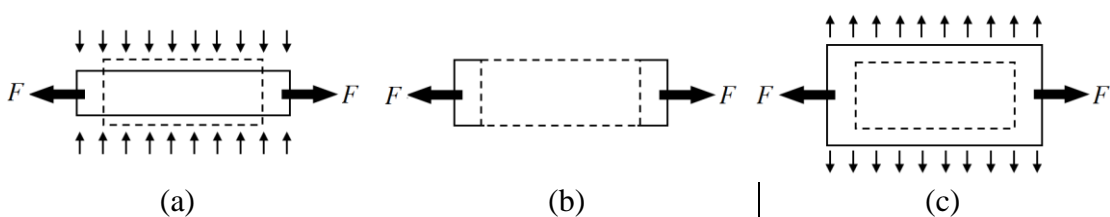


Figure 1.2 Schematic behavior of material with (a) PPR, (b) ZPR and (c) NPR [25]

The pioneer study on engineering mechanics of NPR was published by Love [26], who presented a material with Poisson's ratio of -0.14 in two-dimensional (2D) plane. A preliminary work on the fabrication of re-entrant structure from a thermoplastic open cell foam was carried out by Lakes [22], who proposed two different fabrication methods for polymeric and metallic foams in details. The NPR property of auxetic materials offers several advantages such as enhancement of stiffness, energy dissipation, and indentation resistance (Figure 1.3) [25, 27, 28]. An improvement in these properties confers a great potential on the auxetic material to be used in a broad range of applications. The field of auxetic materials in science and engineering applications was practically initiated when the first NPR polyethylene foam was fabricated [29].

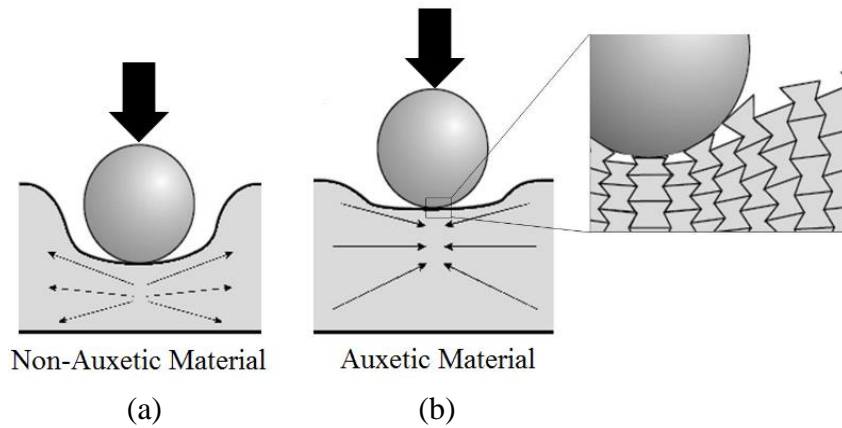


Figure 1.3 Schematic deformation profile (indentation resistance) of (a) non-auxetic and (b) auxetic materials [25]

The classical fabrication process of polymeric auxetic foams includes the following steps: tri-axially compressing of conventional foam, heating the compressed foam then cooling or relaxation operations [30]. Lakes [22] converted a polymeric open-cell foam into an auxetic one by applying one-stage compression to protrude the ribs of each cell inward. The previous process is then followed by heating the foam slightly above its softening temperature to produce re-entrant structures. However, this method has few drawbacks such as severe surface wrinkling of foam and instability in the re-entrant structure. In certain cases, the foam reverts back to the original structure after a long while [30]. Meanwhile, the auxeticity procedure proposed by Lake [22] has been applied by several researchers though with numerous modifications. For

instance, mold lubrication and the use of wires inside the mold for pulling the foam instead of pushing have been suggested to obviate the wrinkling problem [31]. Another way of solving the problem of wrinkles is applying the volumetric compression through several steps to obtain more homogeneous auxetic structures [30].

The use of compressed carbon dioxide [32] to modify the auxeticity process and application of solvents [33] as alternative to the heating stage have been suggested. In addition, replacing the rigid mold with a vacuum bag has also been reported in recent years [34]. Although the conversion process is carried out considering the above-mentioned combination, the modality of either compression or heating process (and/or solvent or carbon dioxide) has a significant impact on the re-entrant structure and mechanical properties of the produced auxetic foams.

1.2 Problem Statement

One of the most important goals of designing an energy absorbing device is to enable maximum energy absorption while the mass is minimal. Hence, cellular materials like foams could be utilized as effective core materials for thin-walled structures to attain a lightweight design [14, 31]. This is due to great energy absorption performance of foam materials as they can endure large deformation at almost constant load. Due to the importance of understanding the crushing characteristics of foam-filled tubes in the field of structural collapse and crashworthy design, a considerable amount of literature has been published on crush analysis of foam-filled thin-walled tubes [15, 17, 35].

During the past 40 years, altering the density of foam fillers were considered as a variable parameter in crashworthiness analysis of foam-filled tubular structures [10, 20]. Variations in the foam density directly affect Young's modulus, plateau stress and most other mechanical properties of foam material than Poisson's ratio. Meanwhile, the effect of foam Poisson's ratio has not been investigated in crush analysis of foam-filled tubular structures as an influencing parameter in determining mechanical deformation and crashworthiness performance of filled structures.

Regarding crush behavior, research information on using auxetic foam with NPR inside the thin-walled tubular structure as an absorber is still limited and sparse, notwithstanding their great potential to be an effective energy absorber.

Despite all modifications done in the auxeticity process, it is obvious that the overall procedure has remained the same, i.e., a volumetric compression of the foam followed by heating and cooling processes. Most established studies in the field of fabrication process concentrate on the heating operation or alternative ways of retaining the primary value of volumetric compression ratio of the foam and minimizing the problem of the foam reverting back to its original size. Meanwhile, the volumetric compression technique suggested by Lakes [22] has not been altered significantly except for the technique proposed by Chan and Evans [30]. The latter study adopted multi-stages volumetric compression ratio technique instead of a single-stage procedure. However, the determined starting densification point (SDP) in one direction was used for the other directions in the compression process. Thus, the wrinkles and creases of the foam surface were minimized but not removed completely. Therefore, more modifications are needed as the mentioned problems -foam instability and surface creasing and wrinkling- still exist. Furthermore, there is no published research on the determination of maximum allowable volumetric compression ratio as an influencing factor in converting process which determines auxeticity level of fabricated foam.

1.3 Research Objectives

The primary objective of this research is to evaluate the crush response and energy absorption performance of auxetic foam-filled tubes when subjected to compressive loading. Owing to the great potential of auxetic foam materials as a filler of thin-wall structures in energy absorption applications, an effort was made to improve the quality of the auxetic foam by employing a novel multi-stage compression methodology. Consequently, an optimum densification point for producing optimized auxetic foam in each of the three directions (x , y , z) was determined by a method called Quasi Tri-axial Compression Method (QTCM). Furthermore, the process of

determining heating time was also modified in order to promote long-term stability of fabricated foam with the maximum stress relaxation. This research provides design information on impact behavior and crashworthiness performance of auxetic foam-filled tubes under quasi-static and dynamic loading to facilitate their application in energy absorbing systems.

The specific objectives of this research are briefly outlined as follows;

- i) To determine densification points required for producing an optimum auxetic foam.
- ii) To evaluate the influence of foam re-entrancy on energy absorption capacity and crush response of auxetic foam-filled tubes under quasi-static and dynamic axial loadings.
- iii) To establish the influence of geometrical parameters on the energy absorption performance and deformation modes of auxetic foam-filled tubes.

1.4 Research Scopes

The scopes and limitations of this research are as follows.

- (a) For fabricating auxetic foam, polyurethane (PU) foam materials with densities of 35 kg/m^3 and 45 kg/m^3 were considered due to their availability, accessibility and affordability.
- (b) Square and circular thin-walled tubes were fabricated considering the following dimensions: thickness of 0.8 mm, outer width 26 mm and heights 50 and 60 mm for the square tube and thickness of 1 mm, outer diameter of 38 mm and height of 80 mm for the circular tubes.

- (c) Tensile tests on aluminum tubes were conducted in accordance with ASTM E8M at a loading rate of 1mm/min.
- (d) Tensile and compression tests on conventional and fabricated auxetic foams were performed at a loading speed of 1 mm/min in accordance to ASTM D3574-95 standard.
- (e) Foam Poisson's ratio was determined under compressive strain. Linear Variable Displacement Transducer (LVDT) was utilized to determine the lateral strain of polymeric foam under axial compressive load.
- (f) Measuring the lateral strain of polymeric foam under compressive strain and determining foam Poisson's ratio using Linear Variable Displacement Transducer (LVDT).
- (g) Quasi-static axial crushing tests on the auxetic foam-filled tubes were conducted at a loading rate of 3 mm/min and 60% of original tube length as crushing length.
- (h) Drop weight impact tests on the filled tube specimens was performed at an impact speed of 5 m/s.
- (i) The auxetic foam-filled tubes under quasi-static axial loading was modeled using explicit nonlinear finite element commercial code LS-DYNA.
- (j) The FE models for empty tube, conventional foam-filled tube and auxetic foam-filled tube were validated using the experimental test results obtained in quasi-static loading.
- (k) The influence of effective tube parameters like wall thickness, height, width/diameter and slenderness ratio on energy absorption performance of empty tube, conventional and auxetic foam-filled tubes was evaluated.

1.5 Significance of Research

The present study has generated new design information on the energy absorption performance and crush response of auxetic foam-filled tubes subjected to compressive axial loading conditions. It has also established the effects of material and geometrical parameters such as foam density, foam Poisson's ratio, tube height, wall thickness, tube diameter and tube width on the energy absorption capacity of auxetic foam-filled tubes which enable efficient design of auxetic foam-filled tubes (square and circular cross-sections) as energy absorbing devices.

Practically, information obtained from this study can be employed to develop design guidelines for the use of auxetic foam-filled tubes as efficient energy absorbers, like vehicle protective structures. This will lead to an increase in the level of safety to the occupants of vehicles.

At present, the suggested approach for fabricating auxetic foam with maximum achievable re-entrancy is still limited and sparse. Hence, the proposed Quasi Tri-axial Compression Method (QTCM) can be used to fabricate auxetic foam with maximum auxeticity level. Moreover, by applying this novel methodology, long-term stability was observed for the fabricated auxetic foam due to attainment of maximum stress relaxation.

The auxetic foams developed in this study could potentially be used in numerous applications owing to their enhanced mechanical behavior compared to the conventional ones. From energy absorption point of view, the auxetic foam showed great potential to be used as an energy absorbing device in structural impact applications not limited to vehicular structures.

1.6 Outline of the Thesis

This thesis entails seven chapters which are arranged thus.

Chapter 2 provides a detailed literature review of the work related to the objectives and scopes of this thesis. The fundamental concept of structural crashworthiness, energy absorption characteristics, impact engineering, thin-walled structures, cellular materials and auxetic foam are summarized in this chapter. Furthermore, an investigation into the fabrication process of polymeric auxetic foam and experimental testing of such materials is also discussed.

Chapter 3 details the research methodology used in this study. The detailed description of material testing, quasi-static and dynamic test conditions are given. Moreover, the development of the FE model for conventional and auxetic foam-filled tubes (square and circular cross-sections) under quasi-static axial loading is explained in this chapter.

Chapter 4 describes the initial study on crush response and energy absorption capability of auxetic foam-filled square tube under quasi-static axial loading conditions.

Chapter 5 elaborates the proposed methodology used for producing the auxetic foam with the maximum achievable negative Poisson's ratio.

Chapter 6 discusses the influence of Poisson's ratio of auxetic foam core on crushing characteristic and energy absorption performance of auxetic foam-filled tubes under quasi-static and dynamic loadings. The interaction effect between the fabricated auxetic foam and tube walls is also determined. In addition, a parametric study of the energy absorption response of auxetic foam filled tube under quasi-static loading is presented.

Chapter 7 summarizes the main conclusion and contribution of this study and the future work is eventually proposed.

REFERENCES

1. Abramowicz W, Jones N. Dynamic axial crushing of square tubes. *International Journal of Impact Engineering*. 1984;2(2):179-208.
2. Santosa SP, Wierzbicki T, Hanssen AG, Langseth M. Experimental and numerical studies of foam-filled sections. *International Journal of Impact Engineering*. 2000;24(5):509-34.
3. Langseth M, Hopperstad O, Hanssen A. Crash behaviour of thin-walled aluminium members. *Thin-walled structures*. 1998;32(1-3):127-50.
4. Kusyairi I, Chiron MA, Irawan YS, Himawan HM. Effects of Origami Pattern Crash Box and Rectangular Pattern Crash Box on The Modelling Of MPV Car Structure on Deformation. *Journal of Energy, Mechanical, Material and Manufacturing Engineering*. 2018;3(2):61-8.
5. Zhang X, Wen Z, Zhang H. Axial crushing and optimal design of square tubes with graded thickness. *Thin-Walled Structures*. 2014;84:263-74.
6. Reyes A, Langseth M, Hopperstad OS. Square aluminum tubes subjected to oblique loading. *International Journal of Impact Engineering*. 2003;28(10):1077-106.
7. Nia AA, Parsapour M. Comparative analysis of energy absorption capacity of simple and multi-cell thin-walled tubes with triangular, square, hexagonal and octagonal sections. *Thin-Walled Structures*. 2014;74:155-65.
8. Fan Z, Lu G, Liu K. Quasi-static axial compression of thin-walled tubes with different cross-sectional shapes. *Engineering Structures*. 2013;55:80-9.
9. Hosseinipour S, Daneshi G. Energy absorption and mean crushing load of thin-walled grooved tubes under axial compression. *Thin-walled structures*. 2003;41(1):31-46.
10. Reid SR, Reddy T, Gray M. Static and dynamic axial crushing of foam-filled sheet metal tubes. *International Journal of Mechanical Sciences*. 1986;28(5):295-322.
11. Reddy T, Wall R. Axial compression of foam-filled thin-walled circular tubes. *International Journal of Impact Engineering*. 1988;7(2):151-66.
12. Li Z, Chen R, Lu F. Comparative analysis of crashworthiness of empty and foam-filled thin-walled tubes. *Thin-Walled Structures*. 2018;124:343-9.
13. Dirgantara T, Jusuf A, Kurniati EO, Gunawan L, Putra IS. Crashworthiness analysis of foam-filled square column considering strain rate effect of the foam. *Thin-Walled Structures*. 2018;129:365-80.
14. Hanssen AG, Langseth M, Hopperstad OS. Static and dynamic crushing of square aluminium extrusions with aluminium foam filler. *International Journal of Impact Engineering*. 2000;24(4):347-83.

15. Asavavisithchai S, Slater D, Kennedy A. Effect of tube length on the bucking mode and energy absorption of Al foam-filled tubes. *Journal of materials science*. 2004;39(24):7395-6.
16. Othman A, Abdullah S, Ariffin A, Mohamed N. Investigating the quasi-static axial crushing behavior of polymeric foam-filled composite pultrusion square tubes. *Materials & Design*. 2014;63:446-59.
17. Ahmad Z, Thambiratnam D. Crushing response of foam-filled conical tubes under quasi-static axial loading. *Materials & design*. 2009;30(7):2393-403.
18. Ahmad Z, Thambiratnam D, Tan A. Dynamic energy absorption characteristics of foam-filled conical tubes under oblique impact loading. *International Journal of Impact Engineering*. 2010;37(5):475-88.
19. Mirfendereski L, Salimi M, Ziaei-Rad S. Parametric study and numerical analysis of empty and foam-filled thin-walled tubes under static and dynamic loadings. *International Journal of Mechanical Sciences*. 2008;50(6):1042-57.
20. Onsalung N, Thinvongpituk C, Painthong K. The influence of foam density on specific energy absorption of rectangular steel tubes. *Energy Research Journal*, 1 (2). 2010:135-40.
21. Lu G, Yu T. *Energy absorption of structures and materials*: Elsevier; 2003.
22. Lakes R. Foam structures with a negative Poisson's ratio. *Science*. 1987;235:1038-41.
23. Evans KE, Nkansah M, Hutchinson I, Rogers S. Molecular network design. *Nature*. 1991;353(6340):124.
24. Prawoto Y. Seeing auxetic materials from the mechanics point of view: a structural review on the negative Poisson's ratio. *Computational Materials Science*. 2012;58:140-53.
25. Evans KE, Alderson A. Auxetic materials: functional materials and structures from lateral thinking! *Advanced materials*. 2000;12(9):617-28.
26. Love AEH. *A treatise on the mathematical theory of elasticity*: Cambridge university press; 2013.
27. Bianchi M, Scarpa FL, Smith CW. Stiffness and energy dissipation in polyurethane auxetic foams. *Journal of Materials Science*. 2008;43(17):5851-60.
28. Choi J, Lakes R. Non-linear properties of polymer cellular materials with a negative Poisson's ratio. *Journal of Materials Science*. 1992;27(17):4678-84.
29. Duncan O, Shepherd T, Moroney C, Foster L, Venkatraman P, Winwood K, et al. Review of auxetic materials for sports applications: Expanding options in comfort and protection. *Applied Sciences*. 2018;8(6):941.
30. Chan N, Evans K. Fabrication methods for auxetic foams. *Journal of Materials Science*. 1997;32(22):5945-53.
31. Scarpa F, Pastorino P, Garelli A, Patsias S, Ruzzene M. Auxetic compliant flexible PU foams: static and dynamic properties. *physica status solidi (b)*. 2005;242(3):681-94.

32. Li Y, Zeng C. Room-temperature, near-instantaneous fabrication of auxetic materials with constant Poisson's ratio over large deformation. *Advanced Materials*. 2016;28(14):2822-6.
33. Grima JN, Attard D, Gatt R, Cassar RN. A Novel Process for the Manufacture of Auxetic Foams and for Their re-Conversion to Conventional Form. *Advanced Engineering Materials*. 2009;11(7):533-5.
34. Bianchi M, Scarpa F, Banse M, Smith C. Novel generation of auxetic open cell foams for curved and arbitrary shapes. *Acta Materialia*. 2011;59(2):686-91.
35. Duarte I, Krstulović-Opara L, Dias-de-Oliveira J, Vesenjak M. Axial crush performance of polymer-aluminium alloy hybrid foam filled tubes. *Thin-Walled Structures*. 2019;138:124-36.
36. Ahmad Z. Impact and energy absorption of empty and foam-filled conical tubes: Queensland University of Technology; 2009.
37. Jones N. *Structural impact*: Cambridge university press; 2011.
38. Ambrósio JA, Pereira MFS, da Silva FP. *Crashworthiness of transportation systems: structural impact and occupant protection*: Springer Science & Business Media; 2012.
39. Deb A, Mahendrakumar M, Chavan C, Karve J, Blankenburg D, Storen S. Design of an aluminium-based vehicle platform for front impact safety. *International journal of impact engineering*. 2004;30(8-9):1055-79.
40. Brown J. *Introduction to the basic principles of crashworthiness*. Bedfordshire: Cranfield University. 2002.
41. Sun G, Liu T, Huang X, Zheng G, Li Q. Topological configuration analysis and design for foam filled multi-cell tubes. *Engineering Structures*. 2018;155:235-50.
42. Liu W, Lin Z, Wang N, Deng X. Dynamic performances of thin-walled tubes with star-shaped cross section under axial impact. *Thin-Walled Structures*. 2016;100:25-37.
43. Hanssen AG, Langseth M, Hopperstad OS. Static and dynamic crushing of circular aluminium extrusions with aluminium foam filler. *International Journal of Impact Engineering*. 2000;24(5):475-507.
44. Eyvazian A, Habibi MK, Hamouda AM, Hedayati R. Axial crushing behavior and energy absorption efficiency of corrugated tubes. *Materials & Design (1980-2015)*. 2014;54:1028-38.
45. Zarei H, Kröger M. Multiobjective crashworthiness optimization of circular aluminum tubes. *Thin-walled structures*. 2006;44(3):301-8.
46. Baroutaji A, Sajjia M, Olabi A-G. On the crashworthiness performance of thin-walled energy absorbers: recent advances and future developments. *Thin-Walled Structures*. 2017;118:137-63.
47. Witteman W. Improved vehicle crashworthiness design by control of the energy absorption for different collision situations. Ph D Thesis, University of Technology, Automotive Engineering and Product Design Technology, Eindhoven, The Netherlands. 1999.

48. Gan N, Yao S, Dong H, Xiong Y, Liu D, Pu D. Energy absorption characteristics of multi-frusta configurations under axial impact loading. *Thin-Walled Structures*. 2018;122:147-57.
49. Rahi A. Controlling energy absorption capacity of combined bitubular tubes under axial loading. *Thin-Walled Structures*. 2018;123:222-31.
50. Azarakhsh S, Ghamarian A. Collapse behavior of thin-walled conical tube clamped at both ends subjected to axial and oblique loads. *Thin-Walled Structures*. 2017;112:1-11.
51. Hussein RD, Ruan D, Lu G, Guillow S, Yoon JW. Crushing response of square aluminium tubes filled with polyurethane foam and aluminium honeycomb. *Thin-Walled Structures*. 2017;110:140-54.
52. Nia AA, Hamedani JH. Comparative analysis of energy absorption and deformations of thin walled tubes with various section geometries. *Thin-Walled Structures*. 2010;48(12):946-54.
53. Li G, Xu F, Sun G, Li Q. A comparative study on thin-walled structures with functionally graded thickness (FGT) and tapered tubes withstanding oblique impact loading. *International Journal of Impact Engineering*. 2015;77:68-83.
54. Zhang X, Zhang H. Static and dynamic bending collapse of thin-walled square beams with tube filler. *International Journal of Impact Engineering*. 2018;112:165-79.
55. Nia AA, Khodabakhsh H. The effect of radial distance of concentric thin-walled tubes on their energy absorption capability under axial dynamic and quasi-static loading. *Thin-Walled Structures*. 2015;93:188-97.
56. Karagiozova D, Jones N. Dynamic elastic–plastic buckling of circular cylindrical shells under axial impact. *International Journal of Solids and Structures*. 2000;37(14):2005-34.
57. Montazeri S, Elyasi M, Moradpour A. Investigating the energy absorption, SEA and crushing performance of holed and grooved thin-walled tubes under axial loading with different materials. *Thin-Walled Structures*. 2018;131:646-53.
58. Bai J, Meng G, Wu H, Zuo W. Bending collapse of dual rectangle thin-walled tubes for conceptual design. *Thin-Walled Structures*. 2019;135:185-95.
59. Reid S. Plastic deformation mechanisms in axially compressed metal tubes used as impact energy absorbers. *International Journal of Mechanical Sciences*. 1993;35(12):1035-52.
60. Hussein RD, Ruan D, Lu G, Sbarski I. Axial crushing behaviour of honeycomb-filled square carbon fibre reinforced plastic (CFRP) tubes. *Composite Structures*. 2016;140:166-79.
61. Yin H, Wen G, Hou S, Chen K. Crushing analysis and multiobjective crashworthiness optimization of honeycomb-filled single and bitubular polygonal tubes. *Materials & Design*. 2011;32(8-9):4449-60.
62. Li Z, Lu F. Bending resistance and energy-absorbing effectiveness of empty and foam-filled thin-walled tubes. *Journal of Reinforced Plastics and Composites*. 2015;34(9):761-8.

63. Linul E, Movahedi N, Marsavina L. On the lateral compressive behavior of empty and ex-situ aluminum foam-filled tubes at high temperature. *Materials*. 2018;11(4):554.
64. Aktay L, Toksoy AK, Güden M. Quasi-static axial crushing of extruded polystyrene foam-filled thin-walled aluminum tubes: experimental and numerical analysis. *Materials & design*. 2006;27(7):556-65.
65. Tarlochan F, Samer F, Hamouda A, Ramesh S, Khalid K. Design of thin wall structures for energy absorption applications: enhancement of crashworthiness due to axial and oblique impact forces. *Thin-Walled Structures*. 2013;71:7-17.
66. Fan Z, Lu G, Yu T, Liu K. Axial crushing of triangular tubes. *International Journal of Applied Mechanics*. 2013;5(01):1350008.
67. Abramowicz W, Jones N. Dynamic axial crushing of circular tubes. *International Journal of Impact Engineering*. 1984;2(3):263-81.
68. Abramowicz W, Jones N. Dynamic progressive buckling of circular and square tubes. *International Journal of Impact Engineering*. 1986;4(4):243-70.
69. Al Galib D, Limam A. Experimental and numerical investigation of static and dynamic axial crushing of circular aluminum tubes. *Thin-Walled Structures*. 2004;42(8):1103-37.
70. Abramowicz W. Thin-walled structures as impact energy absorbers. *Thin-Walled Structures*. 2003;41(2-3):91-107.
71. Guillow S, Lu G, Grzebieta R. Quasi-static axial compression of thin-walled circular aluminium tubes. *International Journal of Mechanical Sciences*. 2001;43(9):2103-23.
72. Abramowicz W, Jones N. Transition from initial global bending to progressive buckling of tubes loaded statically and dynamically. *International Journal of Impact Engineering*. 1997;19(5-6):415-37.
73. Jensen Ø, Langseth M, Hopperstad O. Transition between progressive and global buckling of aluminium extrusions. *WIT Transactions on The Built Environment*. 2002;63.
74. Karagiozova D, Alves MI. Transition from progressive buckling to global bending of circular shells under axial impact—Part I: Experimental and numerical observations. *International Journal of Solids and Structures*. 2004;41(5-6):1565-80.
75. Xu S, Ruan D, Lu G. Strength enhancement of aluminium foams and honeycombs by entrapped air under dynamic loadings. *International Journal of Impact Engineering*. 2014;74:120-5.
76. Veale PJ. Investigation of the behavior of open cell aluminum foam. 2010.
77. Chan N, Evans K. Microscopic examination of the microstructure and deformation of conventional and auxetic foams. *Journal of Materials Science*. 1997;32(21):5725-36.
78. Gibson LJ, Ashby MF. *Cellular solids: structure and properties*: Cambridge university press; 1999.

79. Warren W, Kraynik A. Foam mechanics: the linear elastic response of two-dimensional spatially periodic cellular materials. *Mechanics of Materials*. 1987;6(1):27-37.
80. Timoshenko SP, Gere JM. *Theory of elastic stability*. 1961. McGrawHill-Kogakusha Ltd, Tokyo. 1961:109.
81. De Vries D. *Characterization of polymeric foams*. Eindhoven University of Technology. 2009.
82. Ghamarian A, Zarei H, Farsi M, Ariaeifar N. Experimental and numerical crashworthiness investigation of the empty and foam-filled conical tube with shallow spherical caps. *Strain*. 2013;49(3):199-211.
83. Gao Q, Wang L, Wang Y, Wang C. Crushing analysis and multiobjective crashworthiness optimization of foam-filled ellipse tubes under oblique impact loading. *Thin-Walled Structures*. 2016;100:105-12.
84. Reddy T, Al-Hassani S. Axial crushing of wood-filled square metal tubes. *International journal of mechanical sciences*. 1993;35(3-4):231-46.
85. Gameiro C, Cirne J. Dynamic axial crushing of short to long circular aluminium tubes with agglomerate cork filler. *International Journal of Mechanical Sciences*. 2007;49(9):1029-37.
86. Tankara D, Moradi R, Tay YY, Lankarani HM, editors. Energy absorption characteristics of a thin-walled tube filled with carbon nano polyurethane foam and application in car bumper. *ASME 2014 International Mechanical Engineering Congress and Exposition; 2014: American Society of Mechanical Engineers*.
87. Toksoy AK, Güden M. The strengthening effect of polystyrene foam filling in aluminum thin-walled cylindrical tubes. *Thin-walled structures*. 2005;43(2):333-50.
88. Børvik T, Hopperstad OS, Reyes A, Langseth M, Solomos G, Dyngeland T. Empty and foam-filled circular aluminium tubes subjected to axial and oblique quasistatic loading. *International Journal of Crashworthiness*. 2003;8(5):481-94.
89. Gameiro CP, Cirne J. Dynamic axial crushing of short to long circular aluminium tubes with agglomerate cork filler. *International Journal of Mechanical Sciences*. 2007;49(9):1029-37.
90. Yan L, Chouw N, Jayaraman K. Effect of triggering and polyurethane foam-filler on axial crushing of natural flax/epoxy composite tubes. *Materials & Design (1980-2015)*. 2014;56:528-41.
91. Seitzberger M, Rammerstorfer FG, Gradinger R, Degischer H, Blaimschein M, Walch C. Experimental studies on the quasi-static axial crushing of steel columns filled with aluminium foam. *International Journal of Solids and Structures*. 2000;37(30):4125-47.
92. Zarei H, Kröger M. Optimization of the foam-filled aluminum tubes for crush box application. *Thin-Walled Structures*. 2008;46(2):214-21.
93. Santosa S, Wierzbicki T. Crash behavior of box columns filled with aluminum honeycomb or foam. *Computers & Structures*. 1998;68(4):343-67.

94. Young T. On passive strength and friction. Course of lectures on natural philosophy and themechanical arts: lecture. London: Taylor and Walton; 1807.
95. Xiong J, Gu D, Chen H, Dai D, Shi Q. Structural optimization of re-entrant negative Poisson's ratio structure fabricated by selective laser melting. *Materials & Design*. 2017;120:307-16.
96. Wang K, Chang Y-H, Chen Y, Zhang C, Wang B. Designable dual-material auxetic metamaterials using three-dimensional printing. *Materials & Design*. 2015;67:159-64.
97. Shokri Rad M, Prawoto Y, Ahmad Z. Analytical solution and finite element approach to the 3D re-entrant structures of auxetic materials. *Mechanics of Materials*. 2014;74(0):76-87.
98. Love A. A treatise on the mathematical theory of elasticity, Dover Publications. New York. 1944;1.
99. Gibson L, Ashby M, Schajer G, Robertson C, editors. The mechanics of two-dimensional cellular materials. *Proceedings of the Royal Society of London A: Mathematical, Physical and Engineering Sciences*; 1982: The Royal Society.
100. Lakes R. Foam structures with a negative Poisson's ratio. *Science*. 1987;235(4792):1038-40.
101. Evans K, Nkansah M, Hutchinson I. Molecular network design. 1991.
102. Caddock B, Evans K. Microporous materials with negative Poisson's ratios. I. Microstructure and mechanical properties. *Journal of Physics D: Applied Physics*. 1989;22(12):1877.
103. Evans K, Caddock B. Microporous materials with negative Poisson's ratios. II. Mechanisms and interpretation. *Journal of Physics D: Applied Physics*. 1989;22(12):1883.
104. Anurag C, Harsha AS, Anvesh CK. Auxetic materials. *Int J Trends Eng Technol*. 2015;5(2):156-60.
105. Bianchi M, Scarpa F, Smith C. Shape memory behaviour in auxetic foams: mechanical properties. *Acta Materialia*. 2010;58(3):858-65.
106. Smith CW, Grima J, Evans K. A novel mechanism for generating auxetic behaviour in reticulated foams: missing rib foam model. *Acta materialia*. 2000;48(17):4349-56.
107. Cadamagnani F, Frontoni S, Bianchi M, Scarpa F. Compressive uniaxial properties of auxetic open cell PU based foams. *physica status solidi (b)*. 2009;246(9):2118-23.
108. Friis E, Lakes R, Park J. Negative Poisson's ratio polymeric and metallic foams. *Journal of Materials Science*. 1988;23(12):4406-14.
109. Wang Y-C, Lakes R, Butenhoff A. Influence of cell size on re-entrant transformation of negative Poisson's ratio reticulated polyurethane foams. *Cellular Polymers*. 2001;20(6):373-85.
110. Rad MS. Auxetic Structures for Energy Absorption Applications: Universiti Teknologi Malaysia; 2015.

111. Bianchi M, Scarpa F, Smith C, Whittell GR. Physical and thermal effects on the shape memory behaviour of auxetic open cell foams. *Journal of materials science*. 2010;45(2):341.
112. Choi J, Lakes R. Non-linear properties of metallic cellular materials with a negative Poisson's ratio. *Journal of Materials Science*. 1992;27(19):5375-81.
113. Scarpa F, Ciffo L, Yates J. Dynamic properties of high structural integrity auxetic open cell foam. *Smart Materials and Structures*. 2003;13(1):49.
114. Alderson A, Rasburn J, Evans K. Mass transport properties of auxetic (negative Poisson's ratio) foams. *physica status solidi (b)*. 2007;244(3):817-27.
115. Lakes R. No contractile obligations. *Nature*. 1992;358(6389):713.
116. Lakes R. Deformation mechanisms in negative Poisson's ratio materials: structural aspects. *Journal of materials science*. 1991;26(9):2287-92.
117. Rothenburg L, Berlin AA, Bathurst RJ. Microstructure of isotropic materials with negative Poisson's ratio. *Nature*. 1991;354(6353):470.
118. Bezazi A, Scarpa F. Tensile fatigue of conventional and negative Poisson's ratio open cell PU foams. *International Journal of Fatigue*. 2009;31(3):488-94.
119. Bezazi A, Scarpa F. Mechanical behaviour of conventional and negative Poisson's ratio thermoplastic polyurethane foams under compressive cyclic loading. *International Journal of fatigue*. 2007;29(5):922-30.
120. Scarpa F, Bullough W, Lumley P. Trends in acoustic properties of iron particle seeded auxetic polyurethane foam. *Proceedings of the Institution of Mechanical Engineers, Part C: Journal of Mechanical Engineering Science*. 2004;218(2):241-4.
121. Scarpa F, Smith F. Passive and MR fluid-coated auxetic PU foam—mechanical, acoustic, and electromagnetic properties. *Journal of intelligent material systems and structures*. 2004;15(12):973-9.
122. Grima JN. Auxetic metamaterials. Strasbourg, France. 2010.
123. Argatov II, Guinovart-Díaz R, Sabina FJ. On local indentation and impact compliance of isotropic auxetic materials from the continuum mechanics viewpoint. *International Journal of Engineering Science*. 2012;54:42-57.
124. Coenen V, Alderson K. Mechanisms of failure in the static indentation resistance of auxetic carbon fibre laminates. *physica status solidi (b)*. 2011;248(1):66-72.
125. Scarpa F, Yates J, Ciffo L, Patsias S. Dynamic crushing of auxetic open-cell polyurethane foam. *Proceedings of the Institution of Mechanical Engineers, Part C: Journal of Mechanical Engineering Science*. 2002;216(12):1153-6.
126. Mir M, Ali MN, Sami J, Ansari U. Review of mechanics and applications of auxetic structures. *Advances in Materials Science and Engineering*. 2014;2014.
127. Alderson A, Alderson K. Expanding materials and applications: exploiting auxetic textiles. *Technical textiles international*. 2005;14(6):29-34.
128. Alderson A, Alderson K. Auxetic materials. *Proceedings of the Institution of Mechanical Engineers, Part G: Journal of Aerospace Engineering*. 2007;221(4):565-75.

129. Avellaneda M, Swart PJ. Calculating the performance of 1–3 piezoelectric composites for hydrophone applications: an effective medium approach. *The Journal of the Acoustical Society of America*. 1998;103(3):1449-67.
130. Alderson A. A triumph of lateral thought. *Chemistry & Industry*. 1999;17:384-91.
131. Baughman RH, Shacklette JM, Zakhidov AA, Stafström S. Negative Poisson's ratios as a common feature of cubic metals. *Nature*. 1998;392(6674):362.
132. Testing AASf, Materials. Standard test methods for tension testing of metallic materials: ASTM international; 2009.
133. ASTM D. 3574—Standard Test Methods for Flexible Cellular Materials—Slab, Bonded, and Molded Urethane Foams. 2001.
134. Huber A, Gibson L. Anisotropy of foams. *Journal of Materials Science*. 1988;23(8):3031-40.
135. Hallquist J. LS-DYNA Theoretical Manual (Livermore, CA: Livermore Software Technology Corporation). 2006.
136. Boyer HE. Atlas of Stress--strain Curves. ASM International, Metals Park, Ohio 44073, USA, 1987 630. 1987.
137. Boresi AP, Schmidt RJ, Sidebottom OM. Advanced mechanics of materials: Wiley New York et al.; 1985.
138. Ling Y. Uniaxial true stress-strain after necking. *AMP Journal of technology*. 1996;5(1):37-48.
139. Zhang Z, Liu S, Tang Z. Comparisons of honeycomb sandwich and foam-filled cylindrical columns under axial crushing loads. *Thin-Walled Structures*. 2011;49(9):1071-9.
140. Hou S, Liu T, Zhang Z, Han X, Li Q. How does negative Poisson's ratio of foam filler affect crashworthiness? *Materials & Design*. 2015;82:247-59.
141. Shah QH, Topa A. Modeling large deformation and failure of expanded polystyrene crushable foam using LS-DYNA. *Modelling and Simulation in Engineering*. 2014;2014:1.
142. Hanssen A, Hopperstad OS, Langseth M, Ilstad H. Validation of constitutive models applicable to aluminium foams. *International journal of mechanical sciences*. 2002;44(2):359-406.
143. Zangani D, Robinson M, Gibson A. Progressive failure of composite hollow sections with foam-filled corrugated sandwich walls. *Applied Composite Materials*. 2007;14(5-6):325-42.
144. Hallquist JO. LS-DYNA® Keyword User's Manual Volume II Material Models. Livermore, California, USA. 2013.
145. Tarigopula V, Langseth M, Hopperstad OS, Clausen AH. Axial crushing of thin-walled high-strength steel sections. *International Journal of Impact Engineering*. 2006;32(5):847-82.
146. Reid J, Hiser N. Friction modelling between solid elements. *International Journal of Crashworthiness*. 2004;9(1):65-72.

147. Bala S. Contact modeling in LS-DYNA. Livermore Software Technology Corporation. 2001.
148. Baroutaji A. Energy absorption through the lateral collapse of thin-walled single and nested tubes: Dublin City University; 2014.
149. Hallquist JO. LS-DYNA keyword user's manual. Livermore Software Technology Corporation. 2007;970:299-800.
150. Barsotti M. Comparison of FEM and SPH for modeling a crushable foam aircraft arrestor bed. *Aerospace Journal*. 2012.
151. Wu J, Wang Y, Wan Y, Lei H, Yu F, Liu Y, et al. Processing and properties of rigid polyurethane foams based on bio-oils from microwave-assisted pyrolysis of corn stover. *International Journal of Agricultural and Biological Engineering*. 2009;2(1):40-50.
152. Kormin S, Rus A. Fabrication and characterization of polyurethane foam prepared from liquefied oil palm mesocarp fibre with renewable monomer made from waste cooking oil. *Journal of Fundamental and Applied Sciences*. 2018;10(2S):722-44.
153. Shokri Rad M, Ahmad Z. New approach for fabrication of auxetic foam and determination of Poisson's ratio. *Applied Mechanics & Materials*. 2014(695).
154. Lu R, Liu X, Chen S, Hu X, Liu L. Axial crashing analysis for tailor rolled square tubes with axially graded both wall thickness and material strength. *Thin-Walled Structures*. 2017;117:10-24.
155. Thirumal M, Khastgir D, Singha NK, Manjunath B, Naik Y. Effect of foam density on the properties of water blown rigid polyurethane foam. *Journal of applied polymer science*. 2008;108(3):1810-7.
156. Wu J-W, Sung W-F, Chu H-S. Thermal conductivity of polyurethane foams. *International Journal of Heat and Mass Transfer*. 1999;42(12):2211-7.
157. Spathis G, Niaounakis M, Kontou E, Apekis L, Pissis P, Christodoulides C. Morphological changes in segmented polyurethane elastomers by varying the NCO/OH ratio. *Journal of applied polymer science*. 1994;54(7):831-42.
158. Gogoi R, Niyogi UK, Alam MS, Mehra DS. Study of effect of NCO/OH molar ratio and molecular weight of polyol on the physico-mechanical properties of polyurethane plaster cast. *World Applied Sciences Journal*. 2013;21(2):276-83.
159. Kumar A, Gupta RK. *Fundamentals of polymer engineering, revised and expanded*: CRC Press; 2003.
160. Ouellet S, Cronin D, Worswick M. Compressive response of polymeric foams under quasi-static, medium and high strain rate conditions. *Polymer testing*. 2006;25(6):731-43.
161. Critchley R, Corni I, Wharton JA, Walsh FC, Wood RJ, Stokes KR. A review of the manufacture, mechanical properties and potential applications of auxetic foams. *physica status solidi (b)*. 2013;250(10):1963-82.

LIST OF PUBLICATIONS

1. Mohsenizadeh, S., Alipour, R., Rad, M. S., Nejad, A. F., & Ahmad, Z. (2015). Crashworthiness assessment of auxetic foam-filled tube under quasi-static axial loading. *Materials & Design*, 88, 258-268. (Q1-IF 4.525)
2. Mohsenizadeh, S., Ahmad, Z., Alipour, R., Majid, R. A., & Prawoto, Y. (2019). Quasi Tri-Axial Method for the Fabrication of Optimized Polyurethane Auxetic Foams. *physica status solidi (b)*, 1800587. (Q3- IF 1.729)
3. Mohsenizadeh, S., Alipour, R., Ahmad, Z., & Alias, A. (2016). Influence of auxetic foam in quasi-static axial crushing. *International Journal of Materials Research*, 107(10), 916-924. (Q3- IF 0.748)